



1 **Particle Phase State and Aerosol Liquid Water Greatly**
2 **Impact Secondary Aerosol Formation: Insights into Phase**
3 **Transition and Role in Haze Events**

4 Xiangxinyue Meng¹, Zhijun Wu^{1,2*}, Jingchuan Chen¹, Yanting Qiu¹, Taomou Zong¹,
5 Mijung Song³, Jiye Lee⁴, Min Hu^{1,2}

6 ¹ State Key Joint Laboratory of Environmental Simulation and Pollution Control, International Joint
7 Laboratory for Regional Pollution Control, College of Environmental Sciences and Engineering, Peking
8 University, Beijing 100871, China

9 ² Collaborative Innovation Center of Atmospheric Environment and Equipment Technology, Nanjing
10 University of Information Science and Technology, Nanjing 210044, China

11 ³ Department of Earth and Environmental Sciences, Jeonbuk National University, Jeonju, Republic of
12 Korea, 54896

13 ⁴ Department of Environmental Science and Engineering, Ewha Womans University, Seoul, Republic of
14 Korea, 03760

15 **Corresponding author: zhijunwu@pku.edu.cn*

16 **Abstract.** The particle-phase state is crucial for reactive gas uptake, heterogeneous, and
17 multiphase chemical reactions, thereby impacting secondary aerosol formation. This
18 study provides valuable insights into the significance of particle-phase transition and
19 aerosol liquid water (ALW) in winter particulate growth. Our findings reveal that
20 particles predominantly exist as semi-solid or solid during clean winter days with
21 ambient relative humidity (RH) below 30%. However, non-liquid to liquid phase
22 transition occurs when the ALW mass fraction exceeds 15% (dry mass) at transition RH
23 thresholds of 40-60%. During haze episodes, the transformation rates of sulfate and
24 nitrate aerosols rapidly increase through phase transition and increased ALW by 48%
25 and 11%, respectively, resulting in noticeable increases in secondary inorganic aerosols
26 (SIA). The presence of abundant ALW, favored by elevated RH and higher proportion
27 of SIA, facilitates heterogeneous and aqueous processes in liquid particles, leading to a
28 substantial increase in the formation of secondary organic aerosols and elevated aerosol



29 oxidation. Consequently, the overall hygroscopicity parameters exhibit a substantial
30 enhancement with a mean value of 23%. These results highlight phase transition as a
31 key factor initiating the positive feedback loops between ALW and secondary aerosol
32 formation during haze episodes over the North China Plain. Accurate predictions of
33 secondary aerosol formation necessitate explicit consideration of the particle-phase
34 state in chemical transport models.



35 **1 Introduction**

36 Submicron particles are ubiquitous in the nature, having great impacts on climate,
37 visibility, and human health (Shiraiwa et al., 2011; Ravishankara, 1997; Pöschl,
38 2005; Lelieveld et al., 2015; Seinfeld et al., 2016; Hu et al., 2021). Phase state, a key
39 parameter of particles, plays profound roles in the mass transport of reactive molecules
40 between the gas phase and the particle phase (Marshall et al., 2018; Shiraiwa et al.,
41 2011). This, in turn, influences the gas-particle partitioning of semi-volatile materials
42 (Shiraiwa et al., 2013; Li and Shiraiwa, 2019), multiphase reaction rates of chemical
43 species (Zhang et al., 2018; Mu et al., 2018), and even the ice nucleating activities of
44 organic aerosols (OA) (Murray et al., 2010; Knopf and Alpert, 2023). Aerosol liquid
45 water (ALW) contributes a substantial fraction of the mass in sub-micrometer particles
46 on a global basis (Nguyen et al., 2016). Atmospheric particles with the presence of
47 condensed water serve as suspended vessels of multiphase chemical reactions, leading
48 to significant impacts on secondary aerosol formation, particle size growth, and air
49 quality (Wu et al., 2018; Hodas et al., 2014; Liu et al., 2019). Therefore, a comprehensive
50 understanding of particle-phase state and ALW is crucial for better evaluation of the
51 related environmental effects.

52 In the real atmosphere, the particle-phase state varies significantly among solid, semi-
53 solid, and liquid under different conditions, which specifically influenced by ambient
54 relative humidity (RH), temperature, and aerosol chemical composition. For example,
55 the atmospheric particles in the tropical rainforest over central Amazonia, which
56 primarily consisted of secondary organic aerosols (SOA) derived from oxidation of
57 isoprene, were observed to be in liquid state at $RH > 80\%$ (Bateman et al., 2016), but
58 more non-liquid particles occurred with the impact of anthropogenic pollutants
59 (Bateman et al., 2017). Liu et al. (2019) reported that particles with high mass fraction
60 of inorganics and high RH were prone to be liquid in a subtropical coastal megacity.
61 However, non-liquid particles appeared at $RH < 60\%$ in Beijing (Liu et al., 2017).
62 Moisture can drive an RH-induced glass transition in particles, leading to a liquid state



63 and a significant water uptake at high RH in the lower atmosphere (Mikhailov et al.,
64 2009). Moreover, organic aerosols might be in solid state at upper tropospheric
65 temperatures that below about 210 K (Koop et al., 2011). Therefore, the changing
66 features of aerosol composition and ambient RH may alter the ALW and trigger the
67 phase state variation. More studies are needed to clarify the relationship between
68 aerosol composition, particle-phase state, and ALW.

69 After the implementation of “China’s Action Plan for Air Pollution Prevention and
70 Control” in 2013, emissions of primary particulate matter and several gaseous
71 pollutants have greatly reduced. However, the contribution and proportion of secondary
72 inorganic aerosols (SIA) and secondary organic aerosols (SOA) have become
73 increasingly significant (Lei et al., 2021; Wang et al., 2021b), especially during haze
74 episodes in winter. As mentioned, particles changes from solid to liquid with elevated
75 RH conditions during heavy haze episodes (Liu et al., 2017). In liquid particles, the gas-
76 particle mass transfer for reactive gases can be greatly facilitated due to increased
77 diffusion coefficients, and the thermodynamic equilibrium of semi-volatile compounds
78 may be impacted to contribute to secondary aerosol formation (Shiraiwa et al., 2011; Jia
79 et al., 2023). A recent field study by Gkatzelis et al. (2021) pointed out that the gas-to-
80 particle partitioning in liquid particles enhances the uptake of water-soluble gas
81 compounds, resulting in a 15-25% contribution of SOA mass during particulate
82 pollution in Beijing. Many studies have demonstrated that the abundant ALW and high
83 RH condition can greatly impact secondary aerosol formation processes (Xu et al.,
84 2017; Wang et al., 2021a; Gkatzelis et al., 2021). However, there is still a lack of
85 understanding regarding the role of phase state variations in secondary particulate
86 pollution. In this study, we conducted a one-month field campaign in Beijing during
87 winter to investigate the relationship between particle-phase state, ALW, and the
88 chemical and physical processes involved in haze formation.



89 2 Methodology

90 2.1 Instruments and Measurements

91 Field campaigns were conducted in Beijing from 15th December 2020 to 10th January
92 2021 at the Changping campus of Peking University (40°8'N, 116°6'E). A detailed
93 description of the sampling site can be found in previous studies (Wang et al., 2020d).
94 The instruments were situated in the air monitoring laboratory, located on the top floor
95 of the main building. A weather station (Met One Instruments Inc., USA), a suite of
96 automatic gas analyzers (O₃, SO₂, CO and NO_x) from Thermo Scientific and an
97 Aerodyne Quadrupole Aerosol Chemical Speciation Monitor (Q-ACSM) were operated
98 according to standard protocols (Ng et al., 2011) and necessary information as described
99 in Text S1.

100 The particle rebound fraction (f) was measured using a modified three-arm impactor
101 (Bateman et al., 2014) coupled to a condensation particle counter (CPC, model 3772,
102 TSI Inc.) with a time interval of 3 minutes, as described in our previous work (Liu et
103 al., 2017; Meng et al., 2021). The three-arm impactor consisted of three parallel
104 impactors with different designs. One of the impactors had no plate, while the others
105 had plate equipped with an uncoated plate and a grease-coated plate, respectively. The
106 no-plate impactor provided the total throughput rate, while the solid surface of the
107 uncoated plate let particle rebound, and the sticky surface of the grease-coated plate
108 captured all particles that struck it. To measure the f , a valve system with three
109 solenoids and two actuators was used to ensure that the particle populations passing
110 through the three impactors were sequenced and were measured by the CPC. Thus,
111 rebound fraction, f , was defined as:

$$112 \quad f = \frac{N_2 - N_3}{N_1 - N_3} \quad (1)$$

113 where N_1 was the whole particle population, N_2 was the population of particles that did
114 not strike plus the rebounded particles from the impaction plate, and N_3 was the



115 population of particles that did not strike the impaction plate. Prior to measurement, we
116 dried the particles to below 30% RH using a silica gel diffusion dryer. Then, 300 nm
117 mono-disperse particles were selected by a Differential Mobility Analyzer (DMA, TSI
118 model 3080). An RH adjustment system with two RH probes and a Nafion RH
119 conditioner was employed to measure the RH conditions (ambient RH and impactor
120 RH), as well as to adjust the impactor RH to match the real atmospheric RH. Weekly
121 calibrations using standard ammonium sulfate and daily flow check were conducted
122 (Liu et al., 2021; Liu et al., 2019). Typically, $f < 0.2$ or 0.1 are referred to the completely
123 phase transition from non-liquid to liquid state (Pajunoja et al., 2016; Liu et al., 2017).
124 In this study, we consider $f < 0.2$ in the case of liquid state. The time series of f with an
125 initial time resolution is shown in Figure 1, while the data presented in other figures are
126 all displayed as hourly averages.

127 2.2 Data Analysis

128 The mass concentrations of organic, sulfate, nitrate, ammonium, and chloride in non-
129 refractory particles (NR-PM₁) were analyzed using the standard ACSM data analysis
130 software (v.1.5.10). A collection efficiency (CE) of 0.5 was applied to the dataset (Xu
131 et al., 2017; Matthew et al., 2008). Positive matrix factorization (PMF) was performed
132 on the organic mass spectra using the Igor Pro based PMF2.exe algorithm to resolve
133 primary organic aerosols (POA) and SOA factors. The data and error matrices were
134 pretreated following methods from previous studies (Zhang et al., 2011; Zhang et al.,
135 2017). The key diagnostic plots are provided in supplementary (Figure S1-S2).

136 The aerosol liquid water content contributed by inorganics (ALW_{inorg}) in PM₁ was
137 estimated using the ISORROPIA-II thermodynamic model (Fountoukis and Nenes,
138 2007) with input of aerosol chemical composition measured by Q-ACSM. The particles
139 were assumed to be in metastable state, and the reverse mode was used to calculate the
140 ALW_{inorg} due to absence of gaseous HNO₃ and NH₃. Besides, ALW associated with
141 organics (ALW_{org}) was considered using a simplified equation of k -Köhler theory (Guo



142 et al., 2015;Petters and Kreidenweis, 2007):

$$143 \quad ALW_{org} = V_{org} k_{org} \frac{a_w}{1-a_w}, \quad (2)$$

144 where V_{org} is the volume concentration of organics with a typical density of 1.4 g/cm^3
145 (Cerully et al., 2015), k_{org} is the hygroscopicity parameter of the organics, a_w represents
146 the water activity, which is assumed to have the same value as RH. In this study, we
147 used a fixed k_{org} of 0.06 to evaluate ALW_{org} , which was the average value of the overall
148 k_{org} in the consideration of POA and SOA contributions in the total non-refractory
149 organics ($k_{POA} = 0$ and $k_{SOA} = 0.1$) (Wu et al., 2016;Gunthe et al., 2011). However, it
150 should be note that k_{org} has been found to exhibit a positive linear relationship with the
151 aerosol oxidation degree, which varied among species (Chang et al., 2010;Duplissy et
152 al., 2011). f_{44} , the fraction of m/z 44 fragment signal to total organic signal, is widely
153 used to represent the atmospheric aging process of OA species (Ng et al.,
154 2010;Canagaratna et al., 2015). Real-time k_{org} was calculated by the parametrization of
155 $k_{org} = 1.04 \times f_{44} - 0.02$, as reported by Kuang et al. (2020) for the North China Plain
156 (NCP). The predicted real-time k_{org} ranged from 0.13 to 0.24, which was consistent with
157 the variation range reported for winter Beijing (0.06-0.3) (Li et al., 2019;Jin et al., 2020).
158 For fixed k_{org} , the contribution of organics to ALW was $\sim 12\%$ on average during the
159 observation. However, considering the variation of real-time f_{44} , organics were capable
160 to provide more than 30% and 20% of the total ALW mass on average during clean and
161 polluted days, respectively (Figure S3 and Text S2).

162 For a given internal mixture, the overall particle hygroscopicity (k_{total}) was calculated
163 by a simple mixing rule by weighting the hygroscopicity parameters of the components
164 by their volume fractions in the mixture (Petters and Kreidenweis, 2007):

$$165 \quad k_{total} = k_{inorg} \cdot frac_{inorg} + k_{org} \cdot frac_{org}, \quad (3)$$

166 Where $frac_{inorg}$ and $frac_{org}$ are the inorganics and organics volume fractions in NR-PM₁,
167 respectively. Considering the variability in the composition of inorganics and organics,



168 the hygroscopicity parameters of inorganics (k_{inorg}) was weighted by volume fractions.
169 The main form of inorganic species (NH_4NO_3 and $(\text{NH}_4)_2\text{SO}_4$) in the urban atmosphere
170 was considered due to the lower abundance of chloride in NR-PM₁. The volume fraction
171 of each inorganic species was calculated based on the ion-pairing scheme as described
172 in Gysel et al. (2007) with their gravimetric density (1720 kg m^{-3} for NH_4NO_3 and 1769
173 kg m^{-3} for $(\text{NH}_4)_2\text{SO}_4$) (Wu et al., 2016). The hygroscopicity parameters of NH_4NO_3
174 and $(\text{NH}_4)_2\text{SO}_4$ are 0.58 and 0.48, respectively following previous studies (Wu et al.,
175 2016; Jin et al., 2020; Petters and Kreidenweis, 2007). For hygroscopicity parameters of
176 organics (k_{org}), real-time k_{org} were used as above, which effectively captured the
177 characteristics of the investigated area in our study.

178 3 Results and Discussion

179 3.1 Chemical Composition and Phase State of Sub-micrometer Particles

180 Figure 1 shows the time series of meteorological parameters, chemical composition of
181 NR-PM₁, gas pollutants, and particle rebound fraction from December 16, 2020, to
182 January 10, 2021. The average mass concentration of NR-PM₁ was $15.8 \pm 16.8 \mu\text{g m}^{-3}$
183 during the measurement period. During clean periods (NR-PM₁ < $20 \mu\text{g m}^{-3}$), organics
184 dominated the aerosol composition, accounting for ~45% of NR-PM₁ mass. Nitrate,
185 sulfate, and ammonium contributed 20%, 16%, and 16% to total NR-PM₁ on average,
186 respectively (Figure S4). However, several pollution episodes occurred with rapid
187 growth in NR-PM₁ and ALW mass concentration with higher concentrations of NO_x
188 and SO₂, as marked by yellow shadow in Figure 1. These four polluted episodes
189 typically started with ambient RH below 40% and higher O₃ levels (> 30 ppb) and
190 mounted up with stagnant meteorological conditions bringing high RH (> 60% RH)
191 and low surface wind speed (< 3 m/s). This meteorological pattern is commonly
192 observed over the NCP during haze episodes (Sun et al., 2015; Sun et al., 2013). During
193 these polluted episodes, nitrate increased rapidly accounting for an average of 33% of
194 the total NR-PM₁ mass. ALW was minor during clean days, but increased up to 26% in



195 PM_1 during severe polluted episodes with $NR-PM_1 > 80 \mu g m^{-3}$ (Figure S5). The mass
196 concentrations of POA and SOA both increased during these polluted episodes as
197 shown in Figure 1d. Moreover, the mass contribution of SOA to total OA showed an
198 upward trend in particulate mass, indicating the important contribution of secondary
199 formation during haze formation (Figure S6).

200 As shown in Figure 1f, particle rebound fraction, f , varied with ambient RH from 1.0 to
201 ~ 0.0 during the observation, indicating that particles possessed phase transition from
202 non-liquid to liquid state. Similar patterns of particle-phase transition were found for
203 several polluted episodes. Taking P4 as an example, f remained stable at 0.8 with RH =
204 $\sim 20\%$ during the initial period of stagnant conditions, but gradually dropped to ~ 0.1
205 along with the increasing RH and $NR-PM_1$ during the subsequent haze formation. In
206 addition, we collected several $PM_{2.5}$ filter samples to characterize the bulk-phase
207 viscosity during clean and polluted days based on poke-and-flow experiment, as
208 described in our previous study (Song et al., 2022) and Text S3 (indicated by black and
209 red frames in Figure 1f). As shown in Figure S7, the viscosity was proved to be higher
210 than $\sim 10^8 Pa s$ with a mean value of $f > 0.8$ during clean days, indicating that particles
211 existed in a solid or semi-solid state. However, the viscosity was lower than $\sim 10^2 Pa s$
212 with an average $f < 0.2$ under higher RH conditions during polluted days, indicating the
213 liquid state. It should be note that the viscosity measurement captured the bulk-phase
214 viscosity for water soluble components in $PM_{2.5}$ filter samples, but the online
215 measurement of f depicted 300 nm particles representative of accumulation mode
216 particles, which normally contributed the majority fraction of PM_1 . While the
217 differences in chemical composition between $PM_{2.5}$ filter samples and 300 nm particles
218 may introduce uncertainties when comparing the phase state of the targeted aerosols,
219 the viscosity results showed good agreement with the average variation of f during the
220 corresponding period. Further validation is still necessary to compare the two different
221 techniques and will be displayed in our further study. To directly indicate the phase
222 transition from the perspective of viscosity, RH-dependent f was measured for these



223 filter samples with known bulk-phase viscosity (Figure S8 and Text S4). As expected,
224 the decreasing f from >0.8 to 0 covered the transition range from $\sim 10^8$ Pa s to $\sim 10^2$ Pa
225 s, which indicated the consistent behavior of particle rebound and measured bulk-phase
226 viscosity for the investigated aerosols.

227 3.2 Phase Transition Behavior of Sub-micrometer Particles

228 Figure 2a illustrates the frequency distribution of RH. f as a function of RH were plotted
229 in Figure 2b. During the observation, ambient RH was below 30% for more than half
230 of the time with f predominantly exceeding 0.8 under such conditions. When RH
231 increased to ~ 50 -60%, a majority of f dropped to <0.2 along with the increasing NR-
232 PM_1 mass. This means that particles went through a moisture-induced phase transition
233 from non-liquid to liquid during haze formation when RH reached 60%, which aligned
234 with our previous studies (Liu et al., 2017). Notably, some points with higher mass
235 fraction of inorganics ($f_{\text{inorg}} > 0.7$) showed $f < 0.2$ at RH = 40-50%, indicating that
236 particles with higher f_{inorg} were already in a liquid state. Consequently, particles
237 underwent phase transition with a relatively large RH range of 40-60%, exhibiting
238 varying chemical compositions as marked by the red frame.

239 Particle-phase state is known to be sensitive to ALW by its unique plasticizer effect
240 (Koop et al., 2011). In Figure 2d, f as a function of ALW/NR- PM_1 were plotted to
241 represent the relative water uptake of unit mass dry aerosols with corresponding particle
242 rebound behaviors. Figure 2c displays the frequency distribution of three f intervals in
243 each ALW/NR- PM_1 bin. When ALW/NR- $\text{PM}_1 < 5\%$, the frequency of $f > 0.8$ was
244 higher than 0.65, indicating that particles mostly stay in a more viscous non-liquid state
245 with less water uptake capacity. When ALW/NR- PM_1 increased to 5-15%, f gradually
246 decreased from 0.8 to 0.2, suggesting that the total water uptake gradually enhanced
247 and lowered the viscosity to trigger the phase transition within this range. The non-
248 liquid particles were dominant with the frequency of $f=0.2$ -0.8 close to 0.8. When
249 ALW/NR- $\text{PM}_1 > 15\%$, the frequency of $f < 0.2$ dramatically increased from 0.2 to ~ 0.8 ,



250 reaching close to 1.0 at $ALW/NR-PM_1 > 25\%$ with higher particulate mass. This
251 indicates that particles mostly convert to liquid as the mass fraction of ALW surpasses
252 a certain threshold during haze formation. In general, a good correlation between
253 $ALW/NR-PM_1$ and f was observed. $ALW/NR-PM_1$, used as a mass-based hygroscopic
254 growth factor (Chen et al., 2022; Liu et al., 2018), is suitable to quantify the moisture-
255 induced phase transition capacity of atmospheric particles, and a value of 15% can be
256 the sudden change in the case of phase transition from non-liquid to liquid. It is
257 suggested that caution should be exercised when using the above approach to
258 characterize the phase state of targeted aerosols, as the measured f was representative
259 of accumulation mode particles that dominated the mass concentration of submicron
260 particles (Seinfeld, 2006).

261 It is interesting to note that several points with $ALW/NR-PM_1 < 5\%$ and $NR-PM_1 > 30$
262 $\mu\text{g}/\text{m}^3$ exhibited lower rebound fraction ($f < 0.4$), which was attributed to the variation
263 of RH background from high RH to low RH during the later stages of the haze episodes,
264 as shown in Figure 2d and Figure S9. This suggests that liquid particles may not turn to
265 be a more viscous semi-solid state in a brief period under dehydration process. There
266 are two possible explanations for this phenomenon. Firstly, the presence of significant
267 amounts of inorganic and organic compounds can alter the humidity conditions for
268 deliquescence and efflorescence (Ushijima et al., 2021; Peckhaus et al., 2012). Secondly,
269 these particles are likely become non-ideal mixing due to drying process that form core-
270 shell structure (Shiraiwa et al., 2013; Ciobanu et al., 2009; Song et al., 2013). Studies
271 have revealed that outer phase may form viscous organic shell to prevent water
272 evaporation (Koop et al., 2011; Shiraiwa et al., 2013; Hodas et al., 2015), thus, the inner
273 phase containing inorganics still keep liquid with residual water. However, it should be
274 note that liquid-liquid phase separation was not optically detected under staged
275 dehydration of filter-based Beijing $PM_{2.5}$ droplets by Song et al. (2022). Instead, they
276 observed abrupt effloresced inorganics at $\sim 30\%$ RH, which was much lower than
277 $(\text{NH}_4)_2\text{SO}_4$ and NH_4NO_3 in pure form (Peng et al., 2022). This supports that



278 atmospheric particles are more likely to be metastable after liquification only if RH
279 decreases to very low values.

280 3.3 Effects of Phase Transition and ALW on SIA Formation during Haze Episodes

281 We investigated the f and secondary aerosols during four polluted episodes (P1 to P4)
282 under stagnant weather conditions with $WS < 3 \text{ ms}^{-1}$. Sulfur and nitrogen oxidation
283 ratios, SOR ($nSO_4/(nSO_4 + nSO_2)$) and NOR ($nNO_3/(nNO_3 + nNO_2)$), commonly
284 used as indicators for secondary inorganic transformation (Li et al., 2017), are plotted
285 as a function of f in Figure 3a and 3b. We found that SOR (NOR) remained in a lower
286 level with a mean value of ~ 0.27 (0.08) at $f > 0.2$ for non-liquid particles, but increased
287 significantly to ~ 0.8 (0.35) with increasing ALW/NR- PM_{10} at $f < 0.2$. This indicates that
288 the secondary formation of SIA is facilitated to a certain degree through phase transition
289 and the increasingly higher ALW mass. It should be note that particles can be non-liquid
290 during haze episodes with $f = 1.0-0.2$. Interestingly, SOR and NOR remained in lower
291 levels and did not show notable increase between $f = 1.0-0.8$ and $f = 0.8-0.2$, until
292 particles accomplished the phase transition at $f = 0.2-0.0$ (Figure 3c1 and 3c2). As a
293 result, the median SOR (NOR) increased to higher levels with an increment of 48%
294 (11%) via phase transition was observed along with the increase in ALW.

295 From the perspective of phase state, the increasing mass fraction of ALW reduces the
296 viscosity and triggers the phase transition, which have important roles in the gas-
297 particle mass transfer during haze formation. It is suggested that the secondary
298 transformation of SIA is impeded by limited mass transfer between gas and particle
299 phase when particles are not fully converted into liquid state. However, these limited
300 factors disappear or the dominant formation pathway changes after phase transition. As
301 reported in previous studies, ALW facilitates the secondary formation of sulfate and
302 nitrate via the promotion of heterogeneous reactions (e.g. SO_2 heterogeneous oxidation,
303 N_2O_5 hydrolysis), gas-particle partitioning of semi-volatile components or aqueous-
304 phase reactions on wet aerosols (Chen et al., 2022; Cheng et al., 2016; Wang et al.,



305 2020b;Liu et al., 2020). However, aqueous-phase oxidation of SO₂ may be constrained
306 before phase transition due to the low diffusivity of multiple oxidants (e.g. O₃, H₂O₂
307 and NO₂) in the particles, and it may become the dominant formation pathway in liquid
308 particles (Ravishankara, 1997;Liu et al., 2020). Additionally, the partitioning of nitrate
309 into particles following Henry's Law may also be facilitated by the increased ALW due
310 to enhanced diffusivity of dissolved precursors in liquid particles. In Figure 3d, the mass
311 fraction of SIA ($f_{\text{SIA/NR-PM}_1}$) is plotted as a function of f . The $f_{\text{SIA/NR-PM}_1}$, ALW mass
312 concentration, and RH were grouped and averaged corresponding to f bin width of 10%.
313 We found that $f_{\text{SIA/NR-PM}_1}$ remained stable at $f = 1.0-0.4$, but steadily increased from an
314 average of ~ 0.50 to ~ 0.65 with elevated RH levels ($>40\%$) and decreasing f (from 0.4
315 to 0.0). This indicates that SIA formation was limited for non-liquid particles with
316 higher viscosity under lower RH conditions. However, ALW was steadily enhanced by
317 the increasing RH and started to trigger the phase transition, thereby facilitating the
318 SOR and NOR to a larger extent. Therefore, $f_{\text{SIA/NR-PM}_1}$ apparently increased with the
319 increase in ALW at $f = 0.2-0.0$. The presence of more ALW in liquid particles was
320 expected to promote the SIA formation by acting as multiphase reaction vessels (Zheng
321 et al., 2015;Wang et al., 2020a;Wang et al., 2020b).

322 **3.4 Effects of Phase Transition and ALW on SOA Formation during Haze Episodes**

323 In Figure 4a and 4b, the ratio of SOA to POA (SOA/POA) is plotted as a function of f
324 during these four polluted episodes characterized by ALW/NR-PM₁ and f_{44} . For $f = 1.0-$
325 0.2, particles possessed relatively lower SOA/POA values (1-2.5) with ALW/NR-PM₁
326 $<15\%$, which was independent of NR-PM₁ mass concentrations. However, a noticeable
327 increase in SOA/POA and elevated f_{44} values were observed at $f = 0.2-0.0$, accompanied
328 by increasing ALW/NR-PM₁ and NR-PM₁ mass. This indicates that more oxidized SOA
329 was produced in liquid particles through the phase transition and the increasing mass
330 fraction of ALW during haze formation. Interestingly, we observed that these liquid
331 particles were primarily associated with polluted days during the nighttime (Figure
332 S10). For these liquid particles, SOA/POA doubled to ~ 5.5 along with the increasing



333 f_{44} compared to non-liquid particles, suggesting the important roles of phase transition
334 and ALW in promoting the SOA formation through dark reactions during nighttime.
335 From the perspective of phase state, phase transition was directly indicated by the
336 decreasing f during haze formation driving a large decrease in bulk phase viscosity
337 from $>10^8$ Pa s to $<10^2$ Pa s as proved by viscosity measurement, which may enhance
338 the gas-particle mass transfer. ALW reduces the viscosity and triggers the phase
339 transition, thus facilitating the uptake of precursors and oxidants, and potentially
340 altering the reaction pathway (Tillmann et al., 2010; Berkemeier et al., 2016; Li et al.,
341 2018; Zhao et al., 2019).

342 For non-liquid particles, ALW facilitates the SOA formation via partition and
343 heterogeneous uptake of water-soluble organics from gas phase into the particle phase,
344 leading to a rapid increase in SOA along with ALW (Herrmann et al., 2015; Gkatzelis
345 et al., 2021; Lim et al., 2010; El-Sayed et al., 2015). Subsequent aqueous-phase reactions
346 may occur to form oligomers, organosulfates, and nitrogen-containing organics through
347 radical or non-radical reactions (Surratt et al., 2007; Iinuma et al., 2007; Galloway et al.,
348 2009; Lim et al., 2013; Wang et al., 2020c). However, these reactions may be limited in
349 non-liquid particles by the lower diffusivity due to higher viscosity. In contrast, liquid
350 particles provide unstrained mass transfer of necessary oxidants and precursors between
351 gas and particle phase, which is favorable for aqueous-phase processing. It is well
352 known that aqueous-phase processing can contribute more oxidized SOA (Xu et al.,
353 2017; Ervens et al., 2011; Zheng et al., 2023). Recent field studies have demonstrated
354 that oligomers or dicarboxylic acids were enriched in liquid particles from the reactive
355 uptake of methylglyoxal during the severe haze episodes in Beijing (Zheng et al., 2021).
356 These oxidation products formed through aqueous-phase reactions are typically more
357 oxidized and less volatile than those formed through gas phase photochemistry (Ervens
358 et al., 2011), which can be reserved in the particle phase and increased the SOA mass
359 in total OA. Therefore, the significant growth of SOA/POA and f_{44} after phase transition
360 is attributed by the enhanced heterogeneous or aqueous-phase reactions in liquid



361 particles with abundant ALW during the nighttime.

362 **3.5 Positive Feedback Loops between ALW and Secondary Aerosol Formation**

363 **Triggered by Phase Transition during Haze Episodes**

364 In Figure 5a, the relationship between k_{total} and RH is displayed. The k_{total} , ALW, and
365 NR-PM₁ mass were grouped and averaged corresponding to an RH bin width of 10%.
366 When RH was below 30%, the averaged k_{total} was ~0.35. However, it increased to 0.39
367 with higher ALW and NR-PM₁ mass at RH =40-60%, and further rose to 0.43 with an
368 average maximum ALW value of 56 $\mu\text{g}/\text{m}^3$ when RH reached 70-80%. This indicates
369 that hygroscopic growth of particulate matter underwent two stages with increasing RH
370 and NR-PM₁ mass, particularly at RH = 40-60% and RH > 70%. From the above
371 discussion, we have demonstrated that the non-liquid to liquid phase transition was
372 triggered by the increased ALW, with a transition RH threshold of 40-60% during haze
373 episodes (as indicated by gradual color change in Figure 5a). Phase transition facilitated
374 the formation of sulfate and nitrate aerosols, contributing higher proportion of SIA in
375 total particles under higher RH conditions. Notably, this led to a continuous increase in
376 the volume fraction of inorganics with increasing RH (Figure 5b). Besides, k_{inorg} also
377 slightly increased when RH reached 60% due to increased nitrate contribution in total
378 SIA during haze episodes (Figure 5c and Figure S4). This may explain the first
379 enhancement of k_{total} at RH = 40-60%, which was mainly driven by the large increase
380 in $frac_{inorg}$ favored by phase transition.

381 Furthermore, the increase in k_{total} , coupled with elevated RH levels, led to a greater
382 abundance of ALW mass. Heterogeneous or aqueous-phase reactions were favored with
383 increasing ALW, promoting the formation of more oxidized SOA in liquid particles. At
384 RH > 70%, the significant increase in k_{org} (~14%) compensated for the negative effect
385 of decreased $frac_{org}$ on the total hygroscopicity contributed by organics ($k_{org} \cdot frac_{org}$),
386 leading to a stable $k_{org} \cdot frac_{org}$ with increasing RH (Figure 5c and Figure S11). This, in
387 turn, coordinated with the increased $frac_{inorg}$, resulting in the second enhancement of



388 k_{total} . As a result, phase transition accompanied by increasing ALW mass triggered a
389 noticeable enhancement in k_{total} with a mean value of 23% during haze episodes. The
390 enhanced water uptake ability of aerosols is expected to contribute more ALW under
391 elevated RH conditions, further facilitating the secondary aerosol formation and
392 deteriorating air quality. These results indicate that the establishment of positive
393 feedback loops between ALW and secondary aerosol formation was triggered by phase
394 transition during haze episodes.

395 **4. Conclusion and atmospheric implications**

396 Our findings revealed that particles predominantly exist as semi-solid or solid during
397 clean winter days with RH below 30%. However, non-liquid to liquid phase transition
398 occurred when the ALW mass fraction surpassed 15% (dry mass) at transition RH
399 thresholds ranging from 40% to 60%. Additionally, we observed a consistent pattern in
400 the non-liquid to liquid phase transition during haze formation, as manifested by both
401 particle-rebound fraction and bulk-phase viscosity measurements. Specifically, the
402 decrease in f from >0.8 to 0 corresponded to a viscosity transition ranging from $\sim 10^8$
403 Pa s to $\sim 10^2$ Pa s. During haze episodes, SOR and NOR rapidly increased through phase
404 transition and increased ALW by 48% and 11%, respectively, resulting in noticeable
405 increases in SIA. The presence of abundant ALW, favored by elevated RH and higher
406 proportion of SIA, facilitates heterogeneous and aqueous processes in liquid particles,
407 leading to a substantial increase in the formation of secondary organic aerosols and
408 elevated aerosol oxidation. As a result, the overall hygroscopicity parameters exhibit a
409 substantial enhancement with a mean value of 23%.

410 In our previous studies, we have revealed the positive feedback loops between ALW
411 and anthropogenic SIA at elevated RH levels during haze formation (Wu et al.,
412 2018; Wang et al., 2020b). The contribution of abundant ALW to SOA production has
413 also been reported in various regions with active anthropogenic emissions, such as the
414 Po Valley in Italy, southeastern U.S., and Beijing, China (Carlton and Turpin,



415 2013;Hodas et al., 2014;Xu et al., 2017). However, we observed that secondary
416 transformation of SIA and SOA was significantly enhanced after phase transition with
417 higher ALW mass during the observation. Our findings indicate that the secondary
418 aerosol formation could be impeded on non-liquid particles due to limited mass transfer
419 between gas and particle phase for relevant reaction components (Ravishankara,
420 1997;Shiraiwa et al., 2011;Abbatt et al., 2012;Ma et al., 2022), whereas it is facilitated
421 in liquid particles. It is therefore recommended that non-liquid to liquid phase transition
422 may be considered to be the kick-off for the positive feedback loops between ALW and
423 secondary aerosol formation during haze events. This can be further supported by the
424 case studies for varying polluted episodes, where episodes with phase transition
425 generally exhibit higher secondary transformation rate of secondary aerosols compared
426 to episodes without phase transition (Figure S12 and Text S5). This mechanism is
427 expected to gain significance in other regions with abundant anthropogenic emissions
428 and high background RH during haze formation.

429 **Author contributions**

430 X.X.Y.M. and Z.J.W. conceived the study. X.X.Y.M. conducted the experiments,
431 analyzed the experimental data, and wrote the manuscript with contributions from
432 Z.J.W., M.J.S., J.Y.L. and M.H. J.C.C. participated in the offline experiments and data
433 analysis. Y.T.Q. and T.M.Z. participated in the field experiments and conducted the
434 filter sampling.

435 **Funding**

436 This work was supported by the Fine Particle Research Initiative in East Asia Considering National
437 Differences (FRIEND) Project through the National Research Foundation of Korea (NRF:
438 2020M3G1A1114537) funded by the Ministry of Science and ICT, Korea.

439 **Acknowledgments**

440 We gratefully acknowledge the assistance of Wenfei Zhu for the technical support on Q-ACSM
441 running and instrument calibration during the campaign.



442 **Competing interests**

443 The authors declare that they have no conflict of interest.

444 **Reference**

- 445 Abbatt, J. P. D., Lee, A. K. Y., and Thornton, J. A.: Quantifying trace gas uptake to tropospheric
446 aerosol: recent advances and remaining challenges, *Chem. Soc. Rev.*, 41, 6555-6581, 2012.
- 447 Bateman, A. P., Belassein, H., and Martin, S. T.: Impactor Apparatus for the Study of Particle
448 Rebound: Relative Humidity and Capillary Forces, *Aerosol Sci. Technol.*, 48, 42-52,
449 10.1080/02786826.2013.853866, 2014.
- 450 Bateman, A. P., Gong, Z. H., Liu, P. F., Sato, B., Cirino, G., Zhang, Y., Artaxo, P., Bertram, A. K., Manzi,
451 A. O., Rizzo, L. V., Souza, R. A. F., Zaveri, R. A., and Martin, S. T.: Sub-micrometre particulate matter
452 is primarily in liquid form over Amazon rainforest, *Nat. Geosci.*, 9, 34-+, 2016.
- 453 Bateman, A. P., Gong, Z. H., Harder, T. H., de Sa, S. S., Wang, B. B., Castillo, P., China, S., Liu, Y. J.,
454 O'Brien, R. E., Palm, B. B., Shiu, H. W., Cirino, G. G., Thalman, R., Adachi, K., Alexander, M. L., Artaxo,
455 P., Bertram, A. K., Buseck, P. R., Gilles, M. K., Jimenez, J. L., Laskin, A., Manzi, A. O., Sedlacek, A.,
456 Souza, R. A. F., Wang, J., Zaveri, R., and Martin, S. T.: Anthropogenic influences on the physical
457 state of submicron particulate matter over a tropical forest, *Atmos. Chem. Phys.*, 17, 1759-1773,
458 2017.
- 459 Berkemeier, T., Steimer, S. S., Krieger, U. K., Peter, T., Pöschl, U., Ammann, M., and Shiraiwa, M.:
460 Ozone uptake on glassy, semi-solid and liquid organic matter and the role of reactive oxygen
461 intermediates in atmospheric aerosol chemistry, *Phys. Chem. Chem. Phys.*, 18, 12662-12674,
462 10.1039/C6CP00634E, 2016.
- 463 Canagaratna, M. R., Jimenez, J. L., Kroll, J. H., Chen, Q., Kessler, S. H., Massoli, P., Hildebrandt Ruiz,
464 L., Fortner, E., Williams, L. R., Wilson, K. R., Surratt, J. D., Donahue, N. M., Jayne, J. T., and Worsnop,
465 D. R.: Elemental ratio measurements of organic compounds using aerosol mass spectrometry:
466 characterization, improved calibration, and implications, *Atmos. Chem. Phys.*, 15, 253-272,
467 10.5194/acp-15-253-2015, 2015.
- 468 Carlton, A. G., and Turpin, B. J.: Particle partitioning potential of organic compounds is highest in
469 the Eastern US and driven by anthropogenic water, *Atmos. Chem. Phys.*, 13, 10203-10214,
470 10.5194/acp-13-10203-2013, 2013.
- 471 Cerully, K. M., Bougiatioti, A., Hite Jr, J. R., Guo, H., Xu, L., Ng, N. L., Weber, R., and Nenes, A.: On
472 the link between hygroscopicity, volatility, and oxidation state of ambient and water-soluble
473 aerosols in the southeastern United States, *Atmos. Chem. Phys.*, 15, 8679-8694, 10.5194/acp-15-
474 8679-2015, 2015.
- 475 Chang, R. Y. W., Slowik, J. G., Shantz, N. C., Vlasenko, A., Liggio, J., Sjostedt, S. J., Leaitch, W. R., and
476 Abbatt, J. P. D.: The hygroscopicity parameter (κ) of ambient organic aerosol at a field site subject
477 to biogenic and anthropogenic influences: relationship to degree of aerosol oxidation, *Atmos.*
478 *Chem. Phys.*, 10, 5047-5064, 10.5194/acp-10-5047-2010, 2010.
- 479 Chen, Y., Wang, Y., Nenes, A., Wild, O., Song, S. J., Hu, D. W., Liu, D. T., He, J. J., Ruiz, L. H., Apte, J.
480 S., Gunthe, S. S., and Liu, P. F.: Ammonium Chloride Associated Aerosol Liquid Water Enhances
481 Haze in Delhi, India, *Environ. Sci. Technol.*, 56, 7163-7173, 10.1021/acs.est.2c00650, 2022.



- 482 Cheng, Y., Zheng, G., Wei, C., Mu, Q., Zheng, B., Wang, Z., Gao, M., Zhang, Q., He, K., Carmichael,
483 G., Pöschl, U., and Su, H.: Reactive nitrogen chemistry in aerosol water as a source of sulfate during
484 haze events in China, *Sci. Adv.*, 2, e1601530, doi:10.1126/sciadv.1601530, 2016.
- 485 Ciobanu, V. G., Marcolli, C., Krieger, U. K., Weers, U., and Peter, T.: Liquid-Liquid Phase Separation
486 in Mixed Organic/Inorganic Aerosol Particles, *J. Phys. Chem. A*, 113, 10966-10978, 2009.
- 487 Duplissy, J., DeCarlo, P. F., Dommen, J., Alfarra, M. R., Metzger, A., Barmapadimos, I., Prevot, A. S.
488 H., Weingartner, E., Tritscher, T., Gysel, M., Aiken, A. C., Jimenez, J. L., Canagaratna, M. R., Worsnop,
489 D. R., Collins, D. R., Tomlinson, J., and Baltensperger, U.: Relating hygroscopicity and composition
490 of organic aerosol particulate matter, *Atmos. Chem. Phys.*, 11, 1155-1165, 10.5194/acp-11-1155-
491 2011, 2011.
- 492 El-Sayed, M. M. H., Wang, Y. Q., and Hennigan, C. J.: Direct atmospheric evidence for the
493 irreversible formation of aqueous secondary organic aerosol, *Geophys. Res. Lett.*, 42, 5577-5586,
494 10.1002/2015gl064556, 2015.
- 495 Ervens, B., Turpin, B. J., and Weber, R. J.: Secondary organic aerosol formation in cloud droplets
496 and aqueous particles (aqSOA): a review of laboratory, field and model studies, *Atmos. Chem.*
497 *Phys.*, 11, 11069-11102, 10.5194/acp-11-11069-2011, 2011.
- 498 Fountoukis, C., and Nenes, A.: ISORROPIA II: a computationally efficient thermodynamic
499 equilibrium model for K^+ - Ca^{2+} - Mg^{2+} - NH_4^+ - Na^+ - SO_4^{2-} - NO_3^- - Cl^- - H_2O aerosols, *Atmos.*
500 *Chem. Phys.*, 7, 4639-4659, DOI 10.5194/acp-7-4639-2007, 2007.
- 501 Galloway, M. M., Chhabra, P. S., Chan, A. W. H., Surratt, J. D., Flagan, R. C., Seinfeld, J. H., and
502 Keutsch, F. N.: Glyoxal uptake on ammonium sulphate seed aerosol: reaction products and
503 reversibility of uptake under dark and irradiated conditions, *Atmos. Chem. Phys.*, 9, 3331-3345,
504 10.5194/acp-9-3331-2009, 2009.
- 505 Gkatzelis, G. I., Papanastasiou, D. K., Karydis, V. A., Hohaus, T., Liu, Y., Schmitt, S. H., Schlag, P.,
506 Fuchs, H., Novelli, A., Chen, Q., Cheng, X., Broch, S., Dong, H., Holland, F., Li, X., Liu, Y. H., Ma, X. F.,
507 Reimer, D., Rohrer, F., Shao, M., Tan, Z., Taraborrelli, D., Tillmann, R., Wang, H. C., Wang, Y., Wu, Y.
508 S., Wu, Z. J., Zeng, L. M., Zheng, J., Hu, M., Lu, K. D., Hofzumahaus, A., Zhang, Y. H., Wahner, A.,
509 and Kiendler-Scharr, A.: Uptake of Water-soluble Gas-phase Oxidation Products Drives Organic
510 Particulate Pollution in Beijing, *Geophys. Res. Lett.*, 48, ARTN e2020GL091351
511 10.1029/2020GL091351, 2021.
- 512 Gunthe, S. S., Rose, D., Su, H., Garland, R. M., Achtert, P., Nowak, A., Wiedensohler, A., Kuwata, M.,
513 Takegawa, N., Kondo, Y., Hu, M., Shao, M., Zhu, T., Andreae, M. O., and Pöschl, U.: Cloud
514 condensation nuclei (CCN) from fresh and aged air pollution in the megacity region of Beijing,
515 *Atmos. Chem. Phys.*, 11, 11023-11039, 10.5194/acp-11-11023-2011, 2011.
- 516 Guo, H., Xu, L., Bougiatioti, A., Cerully, K. M., Capps, S. L., Hite Jr, J. R., Carlton, A. G., Lee, S. H.,
517 Bergin, M. H., Ng, N. L., Nenes, A., and Weber, R. J.: Fine-particle water and pH in the southeastern
518 United States, *Atmos. Chem. Phys.*, 15, 5211-5228, 10.5194/acp-15-5211-2015, 2015.
- 519 Gysel, M., Crosier, J., Topping, D. O., Whitehead, J. D., Bower, K. N., Cubison, M. J., Williams, P. I.,
520 Flynn, M. J., McFiggans, G. B., and Coe, H.: Closure study between chemical composition and
521 hygroscopic growth of aerosol particles during TORCH2, *Atmos Chem Phys*, 7, 6131-6144, 2007.
- 522 Herrmann, H., Schaefer, T., Tilgner, A., Styler, S. A., Weller, C., Teich, M., and Otto, T.: Tropospheric
523 Aqueous-Phase Chemistry: Kinetics, Mechanisms, and Its Coupling to a Changing Gas Phase,



- 524 Chem. Rev., 115, 4259-4334, 10.1021/cr500447k, 2015.
- 525 Hodas, N., Sullivan, A. P., Skog, K., Keutsch, F. N., Collett, J. L., Decesari, S., Facchini, M. C., Carlton,
526 A. G., Laaksonen, A., and Turpin, B. J.: Aerosol Liquid Water Driven by Anthropogenic Nitrate:
527 Implications for Lifetimes of Water-Soluble Organic Gases and Potential for Secondary Organic
528 Aerosol Formation, Environ. Sci. Technol. , 48, 11127-11136, 2014.
- 529 Hodas, N., Zuend, A., Mui, W., Flagan, R. C., and Seinfeld, J. H.: Influence of particle-phase state
530 on the hygroscopic behavior of mixed organic-inorganic aerosols, Atmos. Chem. Phys. , 15, 5027-
531 5045, 10.5194/acp-15-5027-2015, 2015.
- 532 Hu, S. Y., Zhao, G., Tan, T. Y., Li, C. C., Zong, T. M., Xu, N., Zhu, W. F., and Hu, M.: Current challenges
533 of improving visibility due to increasing nitrate fraction in PM_{2.5} during the haze days in Beijing,
534 China, Environ. Pollut., 290, 2021.
- 535 Iinuma, Y., Muller, C., Berndt, T., Boge, O., Claeys, M., and Herrmann, H.: Evidence for the existence
536 of organosulfates from beta-pinene ozonolysis in ambient secondary organic aerosol, Environ. Sci.
537 Technol., 41, 6678-6683, 10.1021/es070938t, 2007.
- 538 Jia, L., Xu, Y., and Duan, M.: Explosive formation of secondary organic aerosol due to aerosol-fog
539 interactions, Sci. Total Environ., 866, 161338, <https://doi.org/10.1016/j.scitotenv.2022.161338>,
540 2023.
- 541 Jin, X., Wang, Y., Li, Z., Zhang, F., Xu, W., Sun, Y., Fan, X., Chen, G., Wu, H., Ren, J., Wang, Q., and
542 Cribb, M.: Significant contribution of organics to aerosol liquid water content in winter in Beijing,
543 China, Atmos. Chem. Phys., 20, 901-914, 10.5194/acp-20-901-2020, 2020.
- 544 Knopf, D. A., and Alpert, P. A.: Atmospheric ice nucleation, Nat Rev Phys, 5, 203-217,
545 10.1038/s42254-023-00570-7, 2023.
- 546 Koop, T., Bookhold, J., Shiraiwa, M., and Poschl, U.: Glass transition and phase state of organic
547 compounds: dependency on molecular properties and implications for secondary organic aerosols
548 in the atmosphere, Phys. Chem. Chem. Phys., 13, 19238-19255, 10.1039/c1cp22617g, 2011.
- 549 Kuang, Y., He, Y., Xu, W., Zhao, P., Cheng, Y., Zhao, G., Tao, J., Ma, N., Su, H., Zhang, Y., Sun, J.,
550 Cheng, P., Yang, W., Zhang, S., Wu, C., Sun, Y., and Zhao, C.: Distinct diurnal variation in organic
551 aerosol hygroscopicity and its relationship with oxygenated organic aerosol, Atmos. Chem. Phys.,
552 20, 865-880, 10.5194/acp-20-865-2020, 2020.
- 553 Lei, L., Zhou, W., Chen, C., He, Y., Li, Z. J., Sun, J. X., Tang, X., Fu, P. Q., Wang, Z. F., and Sun, Y. L.:
554 Long-term characterization of aerosol chemistry in cold season from 2013 to 2020 in Beijing, China,
555 Environ. Pollut., 268, 2021.
- 556 Lelieveld, J., Evans, J. S., Fnais, M., Giannadaki, D., and Pozzer, A.: The contribution of outdoor air
557 pollution sources to premature mortality on a global scale, Nature, 525, 367-371,
558 10.1038/nature15371, 2015.
- 559 Li, X. X., Song, S. J., Zhou, W., Hao, J. M., Worsnop, D. R., and Jiang, J. K.: Interactions between
560 aerosol organic components and liquid water content during haze episodes in Beijing, Atmos.
561 Chem. Phys., 19, 12163-12174, 2019.
- 562 Li, Y., and Shiraiwa, M.: Timescales of secondary organic aerosols to reach equilibrium at various
563 temperatures and relative humidities, Atmos. Chem. Phys., 19, 5959-5971, 10.5194/acp-19-5959-
564 2019, 2019.
- 565 Li, Y. J., Sun, Y., Zhang, Q., Li, X., Li, M., Zhou, Z., and Chan, C. K.: Real-time chemical
566 characterization of atmospheric particulate matter in China: A review, Atmos. Environ., 158, 270-



- 567 304, <https://doi.org/10.1016/j.atmosenv.2017.02.027>, 2017.
- 568 Li, Z., Smith, K. A., and Cappa, C. D.: Influence of relative humidity on the heterogeneous oxidation
569 of secondary organic aerosol, *Atmos. Chem. Phys.*, 18, 14585–14608, 10.5194/acp-18-14585-
570 2018, 2018.
- 571 Lim, Y. B., Tan, Y., Perri, M. J., Seitzinger, S. P., and Turpin, B. J.: Aqueous chemistry and its role in
572 secondary organic aerosol (SOA) formation, *Atmos. Chem. Phys.*, 10, 10521–10539, 10.5194/acp-
573 10-10521-2010, 2010.
- 574 Lim, Y. B., Tan, Y., and Turpin, B. J.: Chemical insights, explicit chemistry, and yields of secondary
575 organic aerosol from OH radical oxidation of methylglyoxal and glyoxal in the aqueous phase,
576 *Atmos. Chem. Phys.*, 13, 8651–8667, 10.5194/acp-13-8651-2013, 2013.
- 577 Liu, P., Song, M., Zhao, T., Gunthe, S. S., Ham, S., He, Y., Qin, Y. M., Gong, Z., Amorim, J. C., Bertram,
578 A. K., and Martin, S. T.: Resolving the mechanisms of hygroscopic growth and cloud condensation
579 nuclei activity for organic particulate matter, *Nat. Commun.*, 9, 4076, 10.1038/s41467-018-06622-
580 2, 2018.
- 581 Liu, T., Clegg, S. L., and Abbatt, J. P. D.: Fast oxidation of sulfur dioxide by hydrogen peroxide in
582 deliquesced aerosol particles, *Proc. Natl. Acad. Sci. U.S.A.*, 117, 1354–1359,
583 doi:10.1073/pnas.1916401117, 2020.
- 584 Liu, Y., Wu, Z., Wang, Y., Xiao, Y., Gu, F., Zheng, J., Tan, T., Shang, D., Wu, Y., Zeng, L., Hu, M.,
585 Bateman, A. P., and Martin, S. T.: Submicrometer Particles Are in the Liquid State during Heavy
586 Haze Episodes in the Urban Atmosphere of Beijing, China, *Environ. Sci. Technol. Lett.*, 4, 427–432,
587 10.1021/acs.estlett.7b00352, 2017.
- 588 Liu, Y., Wu, Z., Huang, X., Shen, H., Bai, Y., Qiao, K., Meng, X., Hu, W., Tang, M., and He, L.: Aerosol
589 Phase State and Its Link to Chemical Composition and Liquid Water Content in a Subtropical
590 Coastal Megacity, *Environ. Sci. Technol.*, 53, 5027–5033, 10.1021/acs.est.9b01196, 2019.
- 591 Liu, Y. C., Meng, X. X., Wu, Z. J., Huang, D. D., Wang, H. L., Chen, J., Chen, J. C., Zong, T. M., Fang,
592 X., Tan, T. Y., Zhao, G., Chen, S. Y., Zeng, L. W., Guo, S., Huang, X. F., He, L. Y., Zeng, L. M., and Hu,
593 M.: The particle phase state during the biomass burning events, *Sci. Total Environ.*, 792, ARTN
594 148035
10.1016/j.scitotenv.2021.148035, 2021.
- 595 10.1016/j.scitotenv.2021.148035, 2021.
- 596 Ma, W., Zheng, F. X., Zhang, Y. S., Chen, X., Zhan, J. L., Hua, C. J., Song, B. Y., Wang, Z. C., Xie, J. L.,
597 Yan, C., Kulmala, M., and Liu, Y. C.: Weakened Gas-to-Particle Partitioning of Oxygenated Organic
598 Molecules in Liquefied Aerosol Particles, *Environ. Sci. Technol. Lett.*, 10.1021/acs.estlett.2c00556,
599 2022.
- 600 Marshall, F. H., Berkemeier, T., Shiraiwa, M., Nandy, L., Ohm, P. B., Dutcher, C. S., and Reid, J. P.:
601 Influence of particle viscosity on mass transfer and heterogeneous ozonolysis kinetics in aqueous-
602 sucrose-maleic acid aerosol, *Phys. Chem. Chem. Phys.*, 20, 15560–15573, 2018.
- 603 Matthew, B. M., Middlebrook, A. M., and Onasch, T. B.: Collection efficiencies in an Aerodyne
604 Aerosol Mass Spectrometer as a function of particle phase for laboratory generated aerosols,
605 *Aerosol Sci. Technol.*, 42, 884–898, 10.1080/02786820802356797, 2008.
- 606 Meng, X. X. Y., Wu, Z. J., Guo, S., Wang, H., Liu, K. F., Zong, T. M., Liu, Y. C., Zhang, W. B., Zhang,
607 Z., Chen, S. Y., Zeng, L. M., Hallquist, M., Shuai, S. J., and Hu, M.: Humidity-Dependent Phase State
608 of Gasoline Vehicle Emission-Related Aerosols, *Environ. Sci. Technol.*, 55, 832–841, 2021.



- 609 Mikhailov, E., Vlasenko, S., Martin, S. T., Koop, T., and Poschl, U.: Amorphous and crystalline aerosol
610 particles interacting with water vapor: conceptual framework and experimental evidence for
611 restructuring, phase transitions and kinetic limitations, *Atmos. Chem. Phys.*, 9, 9491–9522, 2009.
- 612 Mu, Q., Shiraiwa, M., Octaviani, M., Ma, N., Ding, A. J., Su, H., Lammel, G., Poschl, U., and Cheng, Y.
613 F.: Temperature effect on phase state and reactivity controls atmospheric multiphase chemistry
614 and transport of PAHs, *Sci. Adv.*, 4, 2018.
- 615 Murray, B. J., Wilson, T. W., Dobbie, S., Cui, Z. Q., Al-Jumur, S. M. R. K., Mohler, O., Schnaiter, M.,
616 Wagner, R., Benz, S., Niemand, M., Saathoff, H., Ebert, V., Wagner, S., and Karcher, B.:
617 Heterogeneous nucleation of ice particles on glassy aerosols under cirrus conditions, *Nat. Geosci.*,
618 3, 233–237, 2010.
- 619 Ng, N. L., Canagaratna, M. R., Zhang, Q., Jimenez, J. L., Tian, J., Ulbrich, I. M., Kroll, J. H., Docherty,
620 K. S., Chhabra, P. S., Bahreini, R., Murphy, S. M., Seinfeld, J. H., Hildebrandt, L., Donahue, N. M.,
621 DeCarlo, P. F., Lanz, V. A., Prevot, A. S. H., Dinar, E., Rudich, Y., and Worsnop, D. R.: Organic aerosol
622 components observed in Northern Hemispheric datasets from Aerosol Mass Spectrometry, *Atmos.*
623 *Chem. Phys.*, 10, 4625–4641, 10.5194/acp-10-4625-2010, 2010.
- 624 Ng, N. L., Herndon, S. C., Trimborn, A., Canagaratna, M. R., Croteau, P. L., Onasch, T. B., Sueper, D.,
625 Worsnop, D. R., Zhang, Q., Sun, Y. L., and Jayne, J. T.: An Aerosol Chemical Speciation Monitor
626 (ACSM) for Routine Monitoring of the Composition and Mass Concentrations of Ambient Aerosol,
627 *Aerosol Sci. Technol.*, 45, 780–794, Pii 934555189
- 628 10.1080/02786826.2011.560211, 2011.
- 629 Nguyen, T. K. V., Zhang, Q., Jimenez, J. L., Pike, M., and Carlton, A. G.: Liquid Water: Ubiquitous
630 Contributor to Aerosol Mass, *Environ. Sci. Technol. Lett.*, 3, 257–263, 2016.
- 631 Pajunoja, A., Hu, W. W., Leong, Y. J., Taylor, N. F., Miettinen, P., Palm, B. B., Mikkonen, S., Collins,
632 D. R., Jimenez, J. L., and Virtanen, A.: Phase state of ambient aerosol linked with water uptake and
633 chemical aging in the southeastern US, *Atmos. Chem. Phys.*, 16, 11163–11176, 2016.
- 634 Peckhaus, A., Grass, S., Treuel, L., and Zellner, R.: Deliquescence and Efflorescence Behavior of
635 Ternary Inorganic/Organic/Water Aerosol Particles, *J. Phys. Chem. A*, 116, 6199–6210,
636 10.1021/jp211522t, 2012.
- 637 Peng, C., Chen, L. X. D., and Tang, M. J.: A database for deliquescence and efflorescence relative
638 humidities of compounds with atmospheric relevance, *Fund Res-China*, 2, 578–587,
639 10.1016/j.fmre.2021.11.021, 2022.
- 640 Petters, M. D., and Kreidenweis, S. M.: A single parameter representation of hygroscopic growth
641 and cloud condensation nucleus activity, *Atmos. Chem. Phys.*, 7, 1961–1971, 2007.
- 642 Pöschl, U.: Atmospheric Aerosols: Composition, Transformation, Climate and Health Effects,
643 *Angewandte Chemie International Edition*, 44, 7520–7540, 10.1002/anie.200501122, 2005.
- 644 Ravishankara, A. R.: Heterogeneous and multiphase chemistry in the troposphere, *Science*, 276,
645 1058–1065, 1997.
- 646 Seinfeld, J. H., Bretherton, C., Carslaw, K. S., Coe, H., DeMott, P. J., Dunlea, E. J., Feingold, G., Ghan,
647 S., Guenther, A. B., Kahn, R., Kraucunas, I., Kreidenweis, S. M., Molina, M. J., Nenes, A., Penner, J. E.,
648 Prather, K. A., Ramanathan, V., Ramaswamy, V., Rasch, P. J., Ravishankara, A. R., Rosenfeld, D.,
- 649 Stephens, G., and Wood, R.: Improving our fundamental understanding of the role of aerosol–



650 cloud interactions in the climate system, *Proc. Natl. Acad. Sci. U. S. A.*, 113, 5781-5790,
651 doi:10.1073/pnas.1514043113, 2016.

652 Seinfeld, J. H., and Pandis, S. N.: *Atmospheric Chemistry and Physics: From Air Pollution to Climate*
653 *Change*, Wiley, 2006.

654 Shiraiwa, M., Ammann, M., Koop, T., and Pöschl, U.: Gas uptake and chemical aging of semisolid
655 organic aerosol particles, *Proc. Natl. Acad. Sci. U. S. A.*, 108, 11003-11008,
656 10.1073/pnas.1103045108, 2011.

657 Shiraiwa, M., Zuend, A., Bertram, A. K., and Seinfeld, J. H.: Gas-particle partitioning of atmospheric
658 aerosols: interplay of physical state, non-ideal mixing and morphology, *Phys. Chem. Chem. Phys.*,
659 15, 11441-11453, 2013.

660 Song, M., Jeong, R., Kim, D., Qiu, Y., Meng, X., Wu, Z., Zuend, A., Ha, Y., Kim, C., Kim, H., Gaikwad,
661 S., Jang, K.-S., Lee, J. Y., and Ahn, J.: Comparison of Phase States of PM_{2.5} over Megacities, Seoul
662 and Beijing, and Their Implications on Particle Size Distribution, *Environ. Sci. Technol.*,
663 10.1021/acs.est.2c06377, 2022.

664 Song, M. J., Marcolli, C., Krieger, U. K., Lienhard, D. M., and Peter, T.: Morphologies of mixed
665 organic/inorganic/aqueous aerosol droplets, *Faraday Discuss.*, 165, 289-316, 2013.

666 Sun, Y. L., Wang, Z. F., Fu, P. Q., Yang, T., Jiang, Q., Dong, H. B., Li, J., and Jia, J. J.: Aerosol
667 composition, sources and processes during wintertime in Beijing, China, *Atmos. Chem. Phys.*, 13,
668 4577-4592, 10.5194/acp-13-4577-2013, 2013.

669 Sun, Y. L., Du, W., Wang, Q. Q., Zhang, Q., Chen, C., Chen, Y., Chen, Z. Y., Fu, P. Q., Wang, Z. F.,
670 Gao, Z. Q., and R., W. D.: Real-Time Characterization of Aerosol Particle Composition above the
671 Urban Canopy in Beijing: Insights into the Interactions between the Atmospheric Boundary Layer
672 and Aerosol Chemistry, *Environ. Sci. Technol.*, 2015 v.49 no.19, pp. 11340-11347,
673 10.1021/acs.est.5b02373, 2015.

674 Surratt, J. D., Kroll, J. H., Kleindienst, T. E., Edney, E. O., Claeys, M., Sorooshian, A., Ng, N. L.,
675 Offenberg, J. H., Lewandowski, M., Jaoui, M., Flagan, R. C., and Seinfeld, J. H.: Evidence for
676 organosulfates in secondary organic aerosol, *Environ. Sci. Technol.*, 41, 517-527,
677 10.1021/es062081q, 2007.

678 Tillmann, R., Hallquist, M., Jonsson, Å. M., Kiendler-Scharr, A., Saathoff, H., Iinuma, Y., and Mentel,
679 T. F.: Influence of relative humidity and temperature on the production of pinonaldehyde and OH
680 radicals from the ozonolysis of α -pinene, *Atmos. Chem. Phys.*, 10, 7057-7072, 10.5194/acp-
681 10-7057-2010, 2010.

682 Ushijima, S. B., Huynh, E., Davis, R. D., and Tolbert, M. A.: Seeded Crystal Growth of Internally Mixed
683 Organic-Inorganic Aerosols: Impact of Organic Phase State, *J. Phys. Chem. A*, 125, 8668-8679,
684 10.1021/acs.jpca.1c04471, 2021.

685 Wang, H., Chen, X., Lu, K., Tan, Z., Ma, X., Wu, Z., Li, X., Liu, Y., Shang, D., Wu, Y., Zeng, L., Hu, M.,
686 Schmitt, S., Kiendler-Scharr, A., Wahner, A., and Zhang, Y.: Wintertime N₂O₅ uptake coefficients
687 over the North China Plain, *Sci. Bull.*, 65, 765-774, <https://doi.org/10.1016/j.scib.2020.02.006>,
688 2020a.

689 Wang, J. F., Ye, J. H., Zhang, Q., Zhao, J., Wu, Y. Z., Li, J. Y., Liu, D. T., Li, W. J., Zhang, Y. G., Wu, C.,
690 Xie, C. H., Qin, Y. M., Lei, Y. L., Huang, X. P., Guo, J. P., Liu, P. F., Fu, P. Q., Li, Y. J., Lee, H. C., Choi,
691 H., Zhang, J., Liao, H., Chen, M. D., Sun, Y. L., Ge, X. L., Martin, S. T., and Jacob, D. J.: Aqueous
692 production of secondary organic aerosol from fossil-fuel emissions in winter Beijing haze, *Proc.*



- 693 Natl. Acad. Sci. U.S.A. , 118, 2021a.
- 694 Wang, Y., Chen, Y., Wu, Z. J., Shang, D. J., Bian, Y. X., Du, Z. F., Schmitt, S. H., Su, R., Gkatzelis, G. I.,
695 Schlag, P., Hohaus, T., Voliotis, A., Lu, K. D., Zen, L. M., Zhao, C. S., Alfara, M. R., McFiggans, G.,
696 Wiedensohler, A., Kiendler-Scharr, A., Zhang, Y. H., and Hu, M.: Mutual promotion between aerosol
697 particle liquid water and particulate nitrate enhancement leads to severe nitrate-dominated
698 particulate matter pollution and low visibility, *Atmos. Chem. Phys.*, 20, 2161-2175, 2020b.
- 699 Wang, Y., Hu, M., Wang, Y.-C., Li, X., Fang, X., Tang, R., Lu, S., Wu, Y., Guo, S., Wu, Z., Hallquist, M.,
700 and Yu, J. Z.: Comparative Study of Particulate Organosulfates in Contrasting Atmospheric
701 Environments: Field Evidence for the Significant Influence of Anthropogenic Sulfate and NO_x,
702 *Environ. Sci. Technol. Lett.*, 7, 787-794, 10.1021/acs.estlett.0c00550, 2020c.
- 703 Wang, Y. J., Hu, M., Wang, Y. C., Li, X., Fang, X., Tang, R. Z., Lu, S. H., Wu, Y. S., Guo, S., Wu, Z. J.,
704 Hallquist, M., and Yu, J. Z.: Comparative Study of Particulate Organosulfates in Contrasting
705 Atmospheric Environments: Field Evidence for the Significant Influence of Anthropogenic Sulfate
706 and NO_x, *Environ. Sci. Technol. Lett.*, 7, 787-794, 10.1021/acs.estlett.0c00550, 2020d.
- 707 Wang, Y. Y., Li, Z. Q., Wang, Q. Y., Jin, X. A., Yan, P., Cribb, M., Li, Y. A., Yuan, C., Wu, H., Wu, T.,
708 Ren, R. M., and Cai, Z. X.: Enhancement of secondary aerosol formation by reduced anthropogenic
709 emissions during Spring Festival 2019 and enlightenment for regional PM_{2.5} control in Beijing,
710 *Atmos. Chem. Phys.*, 21, 915-926, 2021b.
- 711 Wu, Z. J., Zheng, J., Shang, D. J., Du, Z. F., Wu, Y. S., Zeng, L. M., Wiedensohler, A., and Hu, M.:
712 Particle hygroscopicity and its link to chemical composition in the urban atmosphere of Beijing,
713 China, during summertime, *Atmos. Chem. Phys.*, 16, 1123-1138, 10.5194/acp-16-1123-2016,
714 2016.
- 715 Wu, Z. J., Wang, Y., Tan, T. Y., Zhu, Y. S., Li, M. R., Shang, D. J., Wang, H. C., Lu, K. D., Guo, S., Zeng,
716 L. M., and Zhang, Y. H.: Aerosol Liquid Water Driven by Anthropogenic Inorganic Salts: Implying
717 Its Key Role in Haze Formation over the North China Plain, *Environ. Sci. Technol. Lett.* , 5, 160-166,
718 2018.
- 719 Xu, W. Q., Han, T. T., Du, W., Wang, Q. Q., Chen, C., Zhao, J., Zhang, Y. J., Li, J., Fu, P. Q., Wang, Z.
720 F., Worsnop, D. R., and Sun, Y. L.: Effects of Aqueous-Phase and Photochemical Processing on
721 Secondary Organic Aerosol Formation and Evolution in Beijing, China, *Environ. Sci. Technol.*, 51,
722 762-770, 10.1021/acs.est.6b04498, 2017.
- 723 Zhang, Q., Jimenez, J. L., Canagaratna, M. R., Ulbrich, I. M., Ng, N. L., Worsnop, D. R., and Sun, Y.:
724 Understanding atmospheric organic aerosols via factor analysis of aerosol mass spectrometry: a
725 review, *Anal. Bioanal. Chem.*, 401, 3045-3067, 10.1007/s00216-011-5355-y, 2011.
- 726 Zhang, Y., Chen, Y. Z., Lambe, A. T., Olson, N. E., Lei, Z. Y., Craig, R. L., Zhang, Z. F., Gold, A., Onasch,
727 T. B., Jayne, J. T., Worsnop, D. R., Gaston, C. J., Thornton, J. A., Vizuete, W., Ault, A. P., and Surratt,
728 J. D.: Effect of the Aerosol-Phase State on Secondary Organic Aerosol Formation from the Reactive
729 Uptake of Isoprene-Derived Epoxydiols (IEPDX), *Environ. Sci. Technol. Lett.* , 5, 167-174, 2018.
- 730 Zhang, Y. J., Tang, L. L., Croteau, P. L., Favez, O., Sun, Y. L., Canagaratna, M. R., Wang, Z., Couvidat,
731 F., Albinet, A., Zhang, H. L., Sciare, J., Prevot, A. S. H., Jayne, J. T., and Worsnop, D. R.: Field
732 characterization of the PM_{2.5} Aerosol Chemical Speciation Monitor: insights into the composition,
733 sources, and processes of fine particles in eastern China, *Atmos. Chem. Phys.*, 17, 14501-14517,
734 10.5194/acp-17-14501-2017, 2017.
- 735 Zhao, Z., Xu, Q., Yang, X., and Zhang, H.: Heterogeneous Ozonolysis of Endocyclic Unsaturated

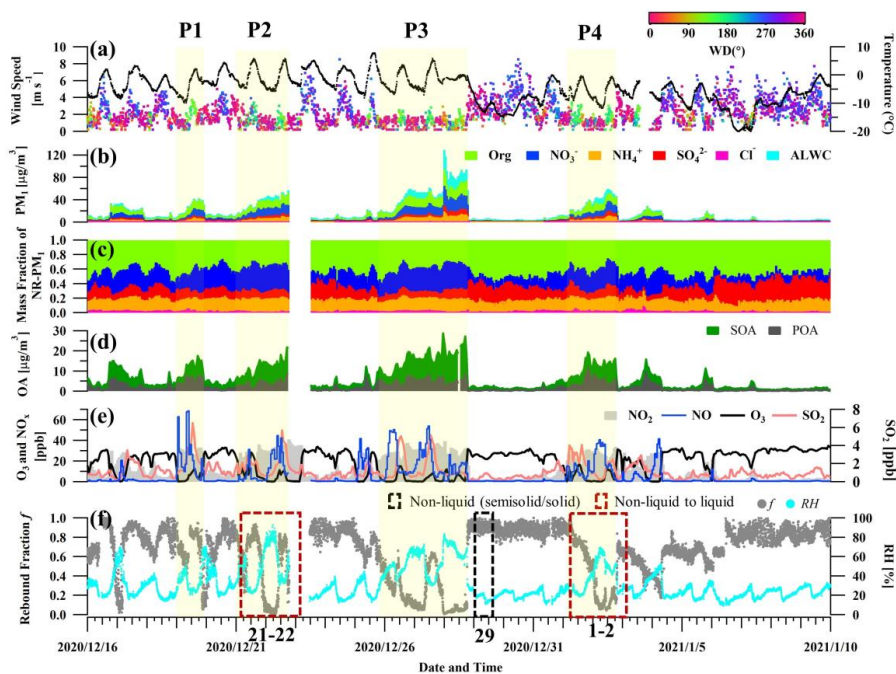


736 Organic Aerosol Proxies: Implications for Criegee Intermediate Dynamics and Later-Generation
737 Reactions, *ACS Earth Space Chem.*, 3, 344-356, 10.1021/acsearthspacechem.8b00177, 2019.
738 Zheng, B., Zhang, Q., Zhang, Y., He, K. B., Wang, K., Zheng, G. J., Duan, F. K., Ma, Y. L., and Kimoto,
739 T.: Heterogeneous chemistry: a mechanism missing in current models to explain secondary
740 inorganic aerosol formation during the January 2013 haze episode in North China, *Atmos. Chem.*
741 *Phys.*, 15, 2031-2049, 10.5194/acp-15-2031-2015, 2015.
742 Zheng, Y., Chen, Q., Cheng, X., Mohr, C., Cai, J., Huang, W., Shrivastava, M., Ye, P., Fu, P., Shi, X.,
743 Ge, Y., Liao, K., Miao, R., Qiu, X., Koenig, T. K., and Chen, S.: Precursors and Pathways Leading to
744 Enhanced Secondary Organic Aerosol Formation during Severe Haze Episodes, *Environ. Sci.*
745 *Technol.*, 55, 15680-15693, 10.1021/acs.est.1c04255, 2021.
746 Zheng, Y., Miao, R. Q., Zhang, Q., Li, Y. W., Cheng, X., Liao, K. R., Koenig, T. K., Ge, Y. L., Tang, L. Z.,
747 Shang, D. J., Hu, M., Chen, S. Y., and Chen, Q.: Secondary Formation of Submicron and
748 Supermicron Organic and Inorganic Aerosols in a Highly Polluted Urban Area, *J. Geophys. Res.*
749 *Atmos.*, 128, 10.1029/2022jd037865, 2023.

750

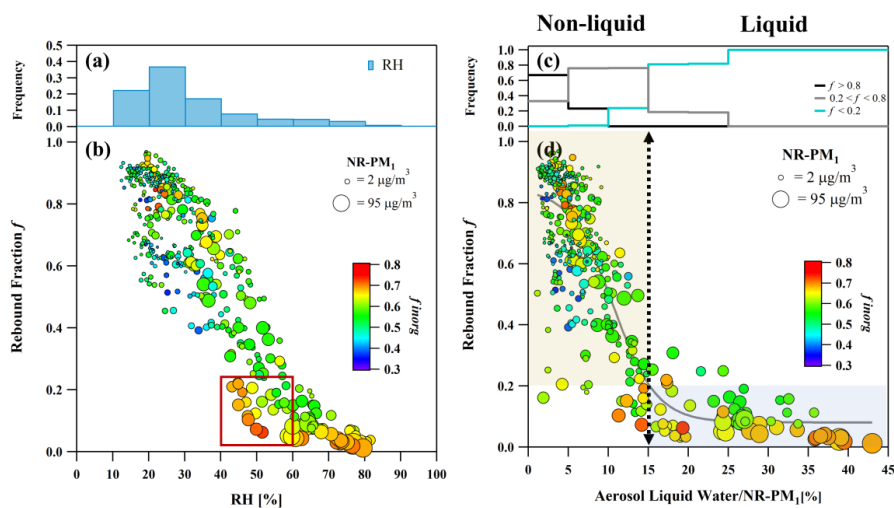


751



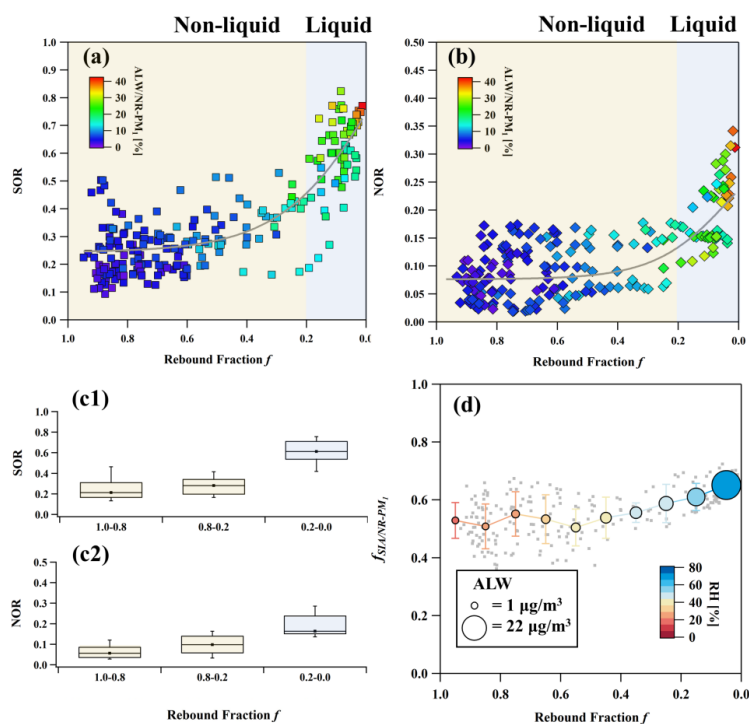
752

753 Figure 1. Time series of (a) wind speed (WS), wind direction (WD) and temperatures,
754 (b) mass concentration of NR-PM₁ and ALW, (c) mass contribution of NR-PM₁, (d)
755 mass concentrations of SOA and POA, (e) concentrations of gas pollutants (NO₂, NO,
756 O₃, and SO₂), (f) rebound fraction and ambient RH during the field campaign. In panel
757 (f), the black (red) frame with dashed line represents the non-liquid state (transition
758 from non-liquid to liquid state) of bulk PM_{2.5} droplets based on off-line viscosity
759 measurement using poke-and-flow technique (Song et al., 2022).



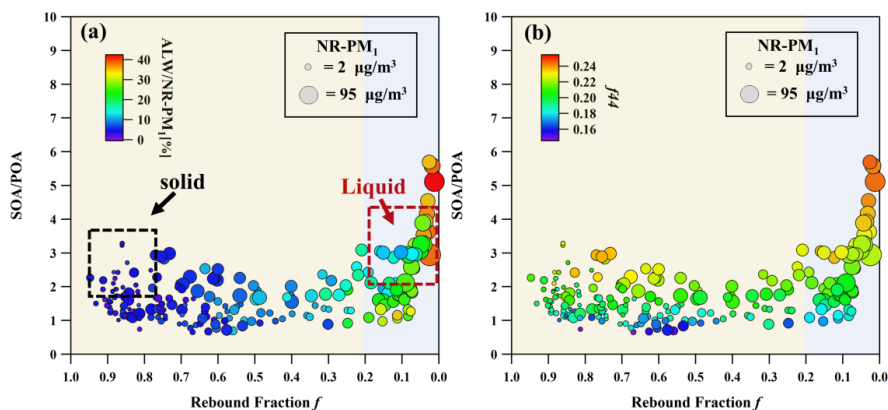
760

761 Figure 2. The frequency distribution of ambient RH in each RH bin (a) and the
762 frequency distribution of each f interval in each ALW/NR-PM₁ bin (c). Rebound
763 fraction f as a function of ambient RH (b) and ALW/NR-PM₁ (d) during the observation.
764 In panel (b) and (d), the scatter points are colored by f_{inorg} in NR-PM₁ and the point size
765 is scaled by NR-PM₁ mass concentration. The yellow and blue shadow represent the
766 non-liquid and liquid phase, respectively.



767

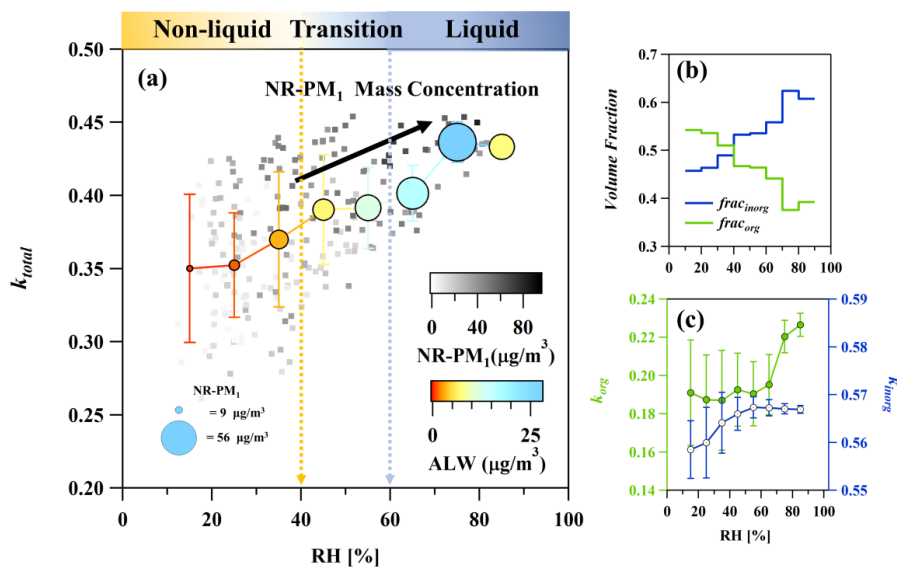
768 Figure 3. SOR and NOR as a function of f (a, b), relationship between SOR or NOR
 769 and three phase transition level (c1, c2), and the mass fraction of SIA in NR-PM₁ as a
 770 function of f during haze episodes (d). Non-liquid particles are marked by yellow
 771 shadows and liquid particles are marked by blue shadows. In panel (a) and (b), the
 772 scatter points are colored by ALW/NR-PM₁ and the trend lines are obtained by sigmoid
 773 fitting. In panel (c1) and (c2), the box plots show 10th, 25th, median, 75th and 90th
 774 percentiles. In panel (d), RH is indicated by color, and ALW mass concentration is
 775 indicated by the size of the circle. The error bars show one standard deviation.



776

777 Figure 4. The relationship between SOA/POA and particle rebound fraction f for phase
 778 transition (a) and oxidation degree (b) during haze episodes. Non-liquid particles are
 779 marked by yellow shadows and liquid particles are marked by blue shadows. The circles
 780 are colored by ALW/NR-PM₁ and f_{44} to represent water uptake capacity and particle
 781 oxidation degree in panel (a) and panel (b), respectively. The sizes of the circles are
 782 scaled to NR-PM₁ mass concentrations. The black (red) frame with dashed line
 783 represent the off-line viscosity measurement results using poke-and-flow technique
 784 corresponding to Figure 1.

785



786

787 Figure 5. The overall hygroscopicity of particles (a), average volume fraction (b) and
788 hygroscopicity (c) of inorganics and organics as a function of RH during haze episodes.
789 k_{total} was calculated using real-time k_{org} . Particles in different phase state condition,
790 including non-liquid, phase transition from non-liquid to liquid, and liquid, are visually
791 distinguished through a gradual color change from yellow to blue, which correlates with
792 RH. In panel (a), the scatter points are colored by NR-PM₁ mass concentrations and
793 averaged in each RH bin. Averaged ALW and NR-PM₁ mass concentrations are
794 indicated by color and the size of the circle, respectively. The error bars show one
795 standard deviation.